

Insulating titanium oxynitride for visible light photocatalysisYuta Aoki,^{1,2,3,*} Masahiro Sakurai,^{4,†} Sinisa Coh,^{3,5,6} James R. Chelikowsky,^{4,7,8} Steven G. Louie,^{3,5}
Marvin L. Cohen,^{3,5} and Susumu Saito^{1,9,10}¹*Department of Physics, Tokyo Institute of Technology, Meguro, Tokyo 152-8551, Japan*²*International Education and Research Center of Science, Tokyo Institute of Technology, Meguro, Tokyo 152-8551, Japan*³*Department of Physics, University of California, Berkeley, California 94720, USA*⁴*Center for Computational Materials, Institute for Computational Engineering and Sciences, The University of Texas at Austin, Austin, Texas 78712, USA*⁵*Materials Sciences Division, Lawrence Berkeley National Laboratory, Berkeley, California 94720, USA*⁶*Department of Mechanical Engineering, Materials Science and Engineering, University of California Riverside, Riverside, California 92521, USA*⁷*Department of Chemical Engineering, The University of Texas at Austin, Austin, Texas 78712, USA*⁸*Department of Physics, The University of Texas at Austin, Austin, Texas 78712, USA*⁹*Advanced Research Center for Quantum Physics and Nanoscience, Tokyo Institute of Technology, Meguro, Tokyo 152-8551, Japan*¹⁰*Materials Research Center for Element Strategy, Tokyo Institute of Technology, Yokohama, Kanagawa 226-8503, Japan*

(Received 20 January 2017; revised manuscript received 7 January 2019; published 25 February 2019)

We propose insulating titanium oxynitrides $\text{Ti}_n\text{N}_2\text{O}_{2n-3}$ as promising water-splitting photocatalytic materials in the visible light range. Using first-principles many-body perturbation theory based on the GW approximation, we show that corundum-type $\text{Ti}_2\text{N}_2\text{O}$ (an example $\text{Ti}_n\text{N}_2\text{O}_{2n-3}$ compound with $n = 2$) has a smaller band gap of about 2.5 eV, which is more suitable to absorb visible light, compared to other Ti-based oxides such as TiO_2 and SrTiO_3 with a band gap of more than 3 eV. Band-gap reduction in $\text{Ti}_2\text{N}_2\text{O}$ is caused by an upward shift of the valence band (negative shift to the oxidation potential of H_2O to O_2) due to the presence of nitrogen $2p$ states. The conduction band is dominated by Ti $3d$ states and the conduction-band minimum is nearly unchanged. As a result, the band-edge potentials of $\text{Ti}_2\text{N}_2\text{O}$ are better aligned to the water reduction and oxidation levels. Our theoretical predictions provide useful insights for the discovery of efficient visible-light-driven photocatalysts for water splitting.

DOI: [10.1103/PhysRevB.99.075203](https://doi.org/10.1103/PhysRevB.99.075203)**I. INTRODUCTION**

Titanium dioxide (TiO_2) is extensively studied as a functional material with the potential of being used in various technological applications such as photocatalysis, photovoltaics, and oxide electronics [1–3]. In particular, triggered by the demonstration of photocatalytic system for water splitting using a rutile TiO_2 anode and Pt cathode [4], numerous efforts have been made to discover TiO_2 -based materials with better photocatalytic performance [5]. Key properties required for water-splitting photocatalytic materials include the magnitude of the band gap and the position of band edges relative to the water reduction and oxidation levels. To ensure the water-splitting reaction without bias voltage, the conduction-band minimum (CBM) needs to be negative (higher in energy) than the $\text{H}_2/\text{H}_2\text{O}$ level of water [usually set to be the normal hydrogen electrode (NHE)], and the valence-band maximum (VBM) needs to be positive (lower in energy) than the $\text{O}_2/\text{H}_2\text{O}$ level (1.23 V vs NHE). A band-gap energy in the visible light range is desirable for utilizing the solar spectrum to induce the water-splitting reaction.

The positions of the band edges of TiO_2 are suitable for water reduction and oxidation, while the band gap of TiO_2 (3.0–3.6 eV in rutile [6–9] and 3.2 eV in anatase [10,11]) is too large to absorb visible light, resulting in poor solar absorption efficiency. To improve the photocatalytic activity of TiO_2 under visible light, there have been continuing efforts to form a band gap suitable for solar-energy absorption as well as the water-splitting reaction. In particular, nitrogen doping into TiO_2 was shown to narrow its band gap, forming an absorption tail in the visible-light region [12–14]. The band-gap narrowing in N-doped TiO_2 can be explained by the schematic band structure shown in Fig. 1. The valence band is composed of hybridized N $2p$ and O $2p$ orbitals. Since the N $2p$ states are higher in energy than the O $2p$ states, VBM is expected to be shifted higher compared to pristine TiO_2 . The conduction band is dominated by empty Ti $3d$ orbitals, being less affected by the dopant. Nitrogen doping is a useful clue to the band-gap engineering of Ti oxides. There is, however, a doping limit in TiO_2 , making it difficult to optimize the photocatalytic performance under visible light. Several studies suggest that the amount of oxygen vacancy in Ti oxide plays a crucial role in controlling the nitrogen concentration [15,16].

Here, we study an alternative way to achieve much higher nitrogen concentrations in Ti oxides. We focus on Ti oxides

*yuta.aoki@nitto.com

†masahiro@ices.utexas.edu

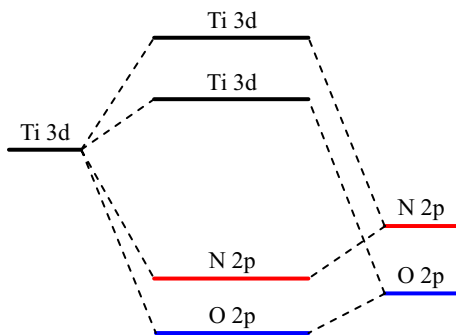


FIG. 1. Schematic band structure of an insulating titanium oxynitride (Ti-N-O compound). The valence band consists mainly of hybridized orbitals from N 2*p* and O 2*p* states, whereas the conduction band is dominated by empty Ti 3*d* orbitals. Octahedral coordination around Ti atoms splits the 3*d* band into lower and upper levels.

with a composition of $\text{Ti}_n\text{O}_{2n-1}$, which can be viewed as oxygen-deficient variants of TiO_2 . Substituting oxygen with nitrogen can yield a series of Ti oxynitrides ($\text{Ti}_n\text{N}_2\text{O}_{2n-3}$). By performing first-principles calculations based on the density-functional theory (DFT) [17,18] and the GW approximation [19], we show that corundum-type $\text{Ti}_2\text{N}_2\text{O}$ (an example $\text{Ti}_n\text{N}_2\text{O}_{2n-3}$ compound with $n = 2$) has a smaller band gap compared to pristine TiO_2 phases. We also show that the band-edge potentials of $\text{Ti}_2\text{N}_2\text{O}$ are much better aligned to the water-splitting levels.

II. COMPUTATIONAL METHODS

The ground-state total energies, the Kohn-Sham eigenfunctions, and corresponding eigenenergies are calculated in the framework of DFT [17,18] as implemented in the QUANTUM ESPRESSO package [20]. We use the generalized gradient approximation (GGA) with the Perdew-Burke-Ernzerhof (PBE) exchange-correlation functional [21]. We employ norm-conserving pseudopotentials [22]. For the Ti pseudopotential, we include semicore 3*s* and 3*p* states as valence states. In generating pseudopotentials, core radii (in a.u.) of 2*s*, 2*p*, 3*s*, 3*p*, and 3*d* states are set to be 1.05, 1.05, 0.90, 0.90, and 1.00, respectively. Wave functions are expanded by a plane-wave basis set with a cutoff energy of 160 Ry in order to get a DFT band gap converged to better than 10 meV. Brillouin-zone integration is performed using the Monkhorst-Pack method [23] with $5 \times 5 \times 8$ and $5 \times 5 \times 5$ *k*-point grids for rutile TiO_2 and anatase TiO_2 , respectively. For metallic corundum Ti_2O_3 , we use a $5 \times 5 \times 5$ *k*-point grid and a Gaussian smearing with a 0.01-Ry spreading. For corundum-type $\text{Ti}_2\text{N}_2\text{O}$, a $5 \times 5 \times 5$ ($5 \times 5 \times 2$) *k*-point grid is used for calculations with a primitive unit cell (hexagonal conventional cell). Atomic positions are optimized by using the Broyden-Fletcher-Goldfarb-Shanno (BFGS) algorithm [24–26].

Quasiparticle band structures are calculated by the “one-shot” GW approach combined with the generalized plasmon-pole model [19,27] as implemented in the BERKELEYGW code [28]. Our GW calculations are performed on top of the eigenvalues and eigenfunctions obtained from the above-mentioned DFT calculations. We employ a fine grid for the dielectric screening to achieve convergence of a band-gap energy within

0.01 eV, a $9 \times 9 \times 15$ grid for rutile TiO_2 , an $8 \times 8 \times 8$ grid for anatase TiO_2 , and a $4 \times 4 \times 4$ grid for corundum-type $\text{Ti}_2\text{N}_2\text{O}$. We adopt simple approximate physical orbitals (SAPOs) [29] to get a large number of empty states that are required to compute the polarizability and the self-energy. For rutile TiO_2 and anatase TiO_2 , the polarizability matrices are computed using a total of 2000 bands and a screened Coulomb cutoff energy of 20 Ry, and the self-energy corrections are calculated using 6000 bands. For corundum-type $\text{Ti}_2\text{N}_2\text{O}$, we employ 2000 bands for sums in the polarizability matrices and 4000 bands for sums in the self-energy operators. Summations over empty states in the self-energy corrections are done with a static remainder approach [30].

III. CRYSTAL STRUCTURE

We focus on $\text{Ti}_n\text{O}_{2n-1}$ compounds as starting materials for insulating Ti oxynitrides without introducing a localized state in the energy gap. Figure 2 illustrates the crystal structure of corundum Ti_2O_3 [31], a $\text{Ti}_n\text{O}_{2n-1}$ compound with $n = 2$. Ti ions occupy two thirds of the octahedral interstitial sites, whereas oxygen ions nearly form a hexagonal close-packed structure. In this Ti sesquioxide, each Ti atom is coordinated octahedrally by neighboring six O atoms. $\text{Ti}_n\text{O}_{2n-1}$ compounds with $n \geq 3$ are known as Magnéli phases [32,33], which are characterized by the presence of a “shear plane,” an ordered plane of oxygen vacancies. Most of the $\text{Ti}_n\text{O}_{2n-1}$ compounds are metallic due to partially occupied Ti 3*d* states, while some of the low-temperature phases are found to be semiconducting with a relatively small band gap (~ 0.1 eV) [34].

Nitrogen doping into $\text{Ti}_n\text{O}_{2n-1}$ phases can be an alternative way to design different Ti-N-O compounds. For example, by replacing two out of $2n - 1$ oxygen atoms of $\text{Ti}_n\text{O}_{2n-1}$ compounds with nitrogen, we can construct a series of

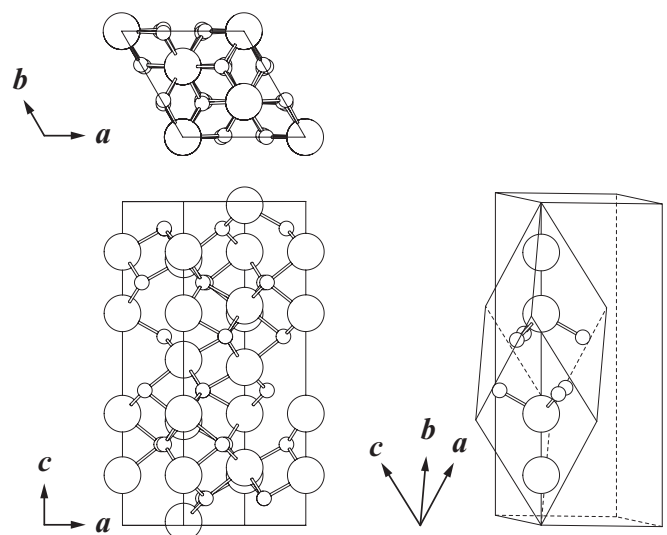


FIG. 2. Crystal structure of corundum Ti_2O_3 . Large and small spheres represent Ti and O atoms, respectively. The hexagonal conventional cell (left) contains six formula units, whereas the rhombohedral primitive cell (right) has two formula units in it. Each Ti atom is surrounded by six O atoms, forming a TiO_6 octahedron.

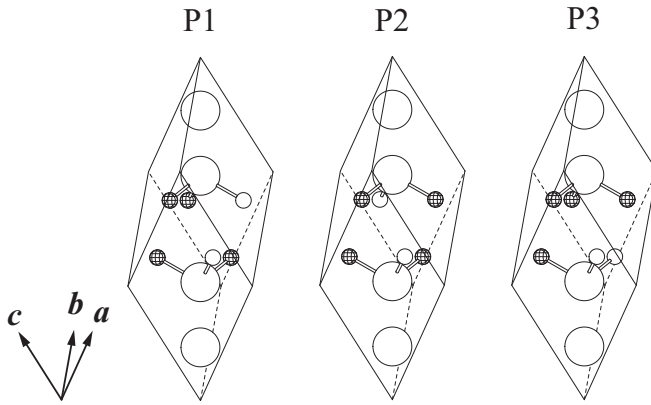


FIG. 3. Crystal structures of corundum-based $\text{Ti}_2\text{N}_2\text{O}$ with different nitrogen-substitution patterns. Large spheres represent Ti atoms. Small spheres with and without a pattern represent N and O atoms, respectively. The structure labeled “P2” has inversion symmetry and the other two structures do not.

Ti oxynitrides $\text{Ti}_n\text{N}_2\text{O}_{2n-3}$ that are expected to have a large insulating gap. With this composition, the resultant materials can keep the stable +IV valency of titanium.

We carry out a case study on compounds with $n = 2$ to demonstrate the feasibility of our concept for different Ti oxynitrides. The primitive unit cell of corundum Ti_2O_3 has two formula units (four Ti atoms and six O atoms) in it. Suppose that four out of six oxygens are substituted with nitrogen to construct a $\text{Ti}_2\text{N}_2\text{O}$ compound (two $\text{Ti}_2\text{N}_2\text{O}$ formula units in a unit cell). There are 15 [=6!/(4!2!)] possibilities for nitrogen-substitution patterns. We actually have only three kinds due to the symmetries of the parent material as shown in Fig. 3. We call them P1, P2, and P3 (P for primitive). We also construct three additional $\text{Ti}_2\text{N}_2\text{O}$ structures using the hexagonal conventional cell that contains six formula units. We call them S1, S2, and S3 (S for supercell). The purpose of constructing S structures is to examine the effect of the disorder (different arrangements of N atoms) on the structural stability of corundum-based $\text{Ti}_2\text{N}_2\text{O}$. We evaluate the formation energy per formula unit of a $\text{Ti}_2\text{N}_2\text{O}$ structure, defined as

$$E = E(\text{Ti}_2\text{N}_2\text{O}) - E(\text{Ti}_2\text{O}_3) - E(\text{N}_2) + E(\text{O}_2). \quad (1)$$

Here, $E(\text{Ti}_2\text{N}_2\text{O})$ and $E(\text{Ti}_2\text{O}_3)$ are the total energies per formula unit of $\text{Ti}_2\text{N}_2\text{O}$ and Ti_2O_3 phases, and $E(\text{N}_2)$ and $E(\text{O}_2)$ are the total energies of N_2 and O_2 molecules, respectively. As shown in Fig. 4, the formation energies of P structures are less than those of S structures. We find that this trend is well correlated with the coordination of titanium atoms with neighboring nitrogen and oxygen atoms. In the P structures, each Ti atom is surrounded by four N atoms and two O atoms, forming a TiN_4O_2 octahedron network. The three S structures have two types of octahedral coordination around the Ti atoms, containing TiN_3O_3 and TiN_6 octahedra. Our total-energy calculations on bulk $\text{Ti}_2\text{N}_2\text{O}$ phases, together with an experimental report [38] on the existence of molecules with a composition $\text{Ti}_2\text{N}_2\text{O}$, provide helpful clues to the synthesis and the stabilization of $\text{Ti}_2\text{N}_2\text{O}$ structures as well as higher $\text{Ti}_n\text{N}_2\text{O}_{2n-3}$ phases. Table I summarizes the structural

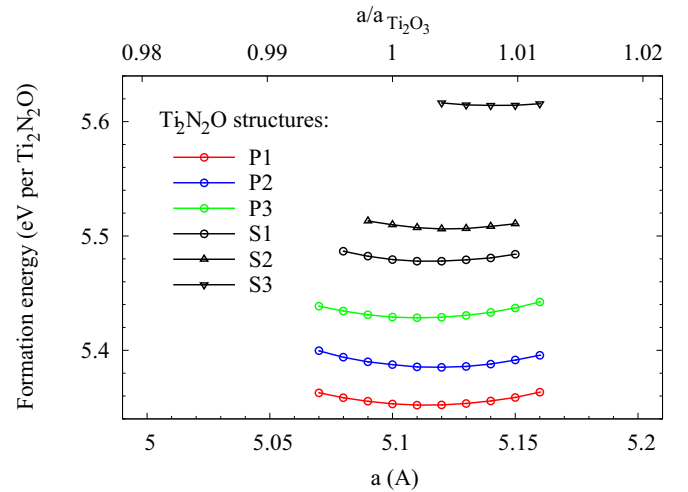


FIG. 4. Formation energies [Eq. (1)] of corundum-based $\text{Ti}_2\text{N}_2\text{O}$ structures (P1–P3 and S1–S3) as a function of lattice constant a . The lattice constant c is optimized at a given a . Atomic positions are relaxed as well.

parameters of corundum-based $\text{Ti}_2\text{N}_2\text{O}$ structures determined by the present DFT-GGA calculations. In Table I, we also list the experimental lattice constants of pristine Ti oxides including corundum Ti_2O_3 .

It has come to our attention that nitrogen doping into $\text{Ti}_n\text{O}_{2n-1}$ compounds with $n \geq 3$ has been studied theoretically [39] and experimentally [40–42]. In particular, Wu and his co-workers used a high throughput screening method within DFT [39]. They find that $\text{Ti}_3\text{N}_2\text{O}_3$ (the $n = 3$ case) adopts the crystal structure of Ta_3N_5 , which is almost isomorphic to the α - Ti_3O_5 structure. The band-gap value of $\text{Ti}_3\text{N}_2\text{O}_3$ is estimated to be 2.37 eV within their Δ -sol methods [43]. The material is also predicted to have a favorable band-edge position for water splitting.

IV. ELECTRONIC STRUCTURE

Electronic band structures of corundum Ti_2O_3 and corundum-based $\text{Ti}_2\text{N}_2\text{O}$ phases, calculated by the DFT-GGA and GW methods, are shown in Fig. 5. Since the energies of the P structures are less than those of the S structures (Fig. 4), GW calculations were performed only on the P structures. Corundum Ti_2O_3 , a parent phase of $\text{Ti}_2\text{N}_2\text{O}$ structures, is metallic, being consistent with experimental findings. As shown in Fig. 5(a), the O $2p$ band (fully occupied) and lower Ti $3d$ band (partially occupied) in Ti_2O_3 are separated by an energy gap of 2.85 eV within the DFT. Nitrogen substitution into Ti_2O_3 opens a substantial band gap in the resultant $\text{Ti}_2\text{N}_2\text{O}$ phases [Figs. 5(b)–5(d)], as expected from the electron-counting rule. We find that the P1 and P2 structures are direct-gap semiconductors, while the P3 structure is an indirect-gap semiconductor. Three P structures have no localized state in the energy gap. Through the projected density of states calculations, we have confirmed that the valence band of $\text{Ti}_2\text{N}_2\text{O}$ is composed mainly of N $2p$ and O $2p$ states. Major contributions to the conduction band of $\text{Ti}_2\text{N}_2\text{O}$ are Ti $3d$ states. These results support the realization of our band-engineering concept shown schematically in Fig. 1.

TABLE I. Structural parameters of rutile TiO_2 [space group $P4_2/mmm$ (No. 136), tetragonal], anatase TiO_2 [$I4_1/amd$ (No. 141), tetragonal], corundum Ti_2O_3 [$R\bar{3}c$ (No. 167), trigonal], and corundum-based $\text{Ti}_2\text{N}_2\text{O}$. The atomic positions of $\text{Ti}_2\text{N}_2\text{O}$ structures are given in the Supplemental Material [35].

Material	Method	Lattice constant (\AA)	Atomic positions			
Rutile TiO_2	X-ray [36]	$a = 4.594, c = 2.959$	Ti	$2a$	$(0, 0, 0)$	$v = 0.305$
			O	$4f$	$(v, v, 0)$	
Anatase TiO_2	X-ray [37]	$a = 3.785, c = 9.514$	Ti	$4a$	$(0, 0, 0)$	$v = 0.208$
			O	$8e$	$(0, 0, v)$	
Corundum Ti_2O_3	X-ray [31]	$a = 5.149, c = 13.642$	Ti	$12c$	$(0, 0, \pm u), (0, 0, 1/2 \pm u)$	$u = 0.345$
			O	$18e$	$(\pm v, 0, \pm 1/4), (\pm v, \pm v, \pm 3/4)$	$v = 0.317$
Corundum Ti_2O_3	GGA (this work)	$a = 5.10, c = 14.0$				$u = 0.345, v = 0.312$
$\text{Ti}_2\text{N}_2\text{O}$, P1	GGA (this work)	$a = 5.11, c = 14.1$				
$\text{Ti}_2\text{N}_2\text{O}$, P2	GGA (this work)	$a = 5.12, c = 13.9$				
$\text{Ti}_2\text{N}_2\text{O}$, P3	GGA (this work)	$a = 5.11, c = 14.0$				
$\text{Ti}_2\text{N}_2\text{O}$, S1	GGA (this work)	$a = 5.11, c = 14.0$				
$\text{Ti}_2\text{N}_2\text{O}$, S2	GGA (this work)	$a = 5.12, c = 14.0$				
$\text{Ti}_2\text{N}_2\text{O}$, S3	GGA (this work)	$a = 5.14, c = 14.1$				

Band-gap values of pristine TiO_2 phases (rutile and anatase) and corundum-based $\text{Ti}_2\text{N}_2\text{O}$ structures are summarized in Table II. For calculations on rutile and anatase, we used the experimental lattice constant listed in Table I. The present GW methods give band-gap values of 3.38 eV for rutile TiO_2 and 3.86 eV for anatase TiO_2 , respectively. Our GW band-gap values agree well with previous GW calculations [44–49] and are consistent with experiments [6,9]. This indicates that our GW methods can give a band gap with high accuracy. The calculated band-gap values of corundum-based $\text{Ti}_2\text{N}_2\text{O}$ structures, ranging from 2.42 to 2.62 eV within the GW approximation, are significantly smaller than those of pristine TiO_2 phases.

We estimate the positions of CBM and VBM from the GW calculations relative to the water reduction and oxidation levels using the method proposed in Ref. [50]. In this

method, the average Hartree potential is used as an energy reference for band alignment. For the sake of simplification in calculations for semiconductor-water interfacial systems, this method typically gives the band-edge positions with a mean absolute error of 0.19 eV [50] compared to the experimental data (indicated by an error bar in Fig. 6). Figure 6 shows the band-edge positions estimated for pristine TiO_2 phases (rutile and anatase) and $\text{Ti}_2\text{N}_2\text{O}$ structures. In rutile and anatase, the CBM locates in a nearly optimal way, while the position of the VBM is rather “deep” in comparison to the $\text{O}_2/\text{H}_2\text{O}$ level. In $\text{Ti}_2\text{N}_2\text{O}$ structures, the presence of occupied N $2p$ states brings an upward shift of the VBM, making the VBM closer to the $\text{O}_2/\text{H}_2\text{O}$ level. The positions of the CBM of $\text{Ti}_2\text{N}_2\text{O}$ structures are still within the range of -1 V to the $\text{H}_2/\text{H}_2\text{O}$ level. The estimated band-edge positions of $\text{Ti}_2\text{N}_2\text{O}$ are similar to those of $\text{Ti}_3\text{N}_2\text{O}_3$ (the $n = 3$ case) [39]. The

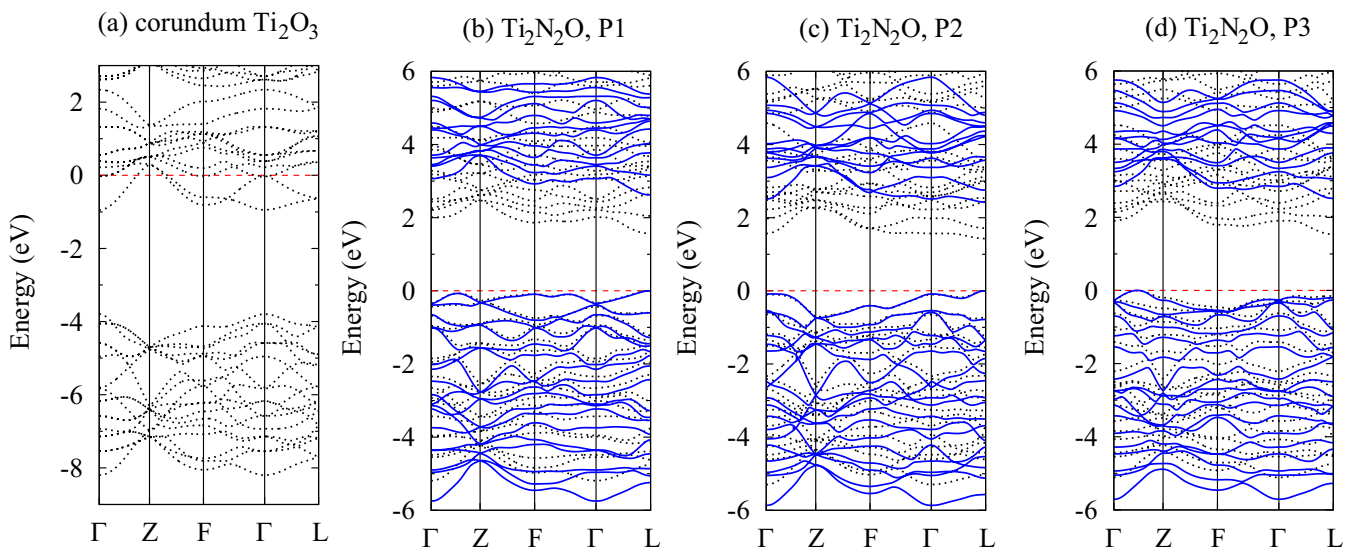


FIG. 5. Band structures of (a) corundum Ti_2O_3 and (b)–(d) corundum-based $\text{Ti}_2\text{N}_2\text{O}$ phases, calculated by GGA (black, dotted) and GW methods (blue, solid). The red dashed line indicates the Fermi level in (a) and the top of the valence band in (b)–(d). The P1 and P2 structures are direct-gap semiconductors, whereas the P3 structure is an indirect-gap semiconductor. In (b)–(d), the GGA and GW results are displayed with the top of the valence band aligned.

TABLE II. Band-gap values in eV, calculated by DFT-GGA and GW methods. Experimental values, determined by photoemission spectroscopy (PES) and optical methods (Opt.), are also listed for comparison.

	TiO ₂		Ti ₂ N ₂ O		
	Rutile	Anatase	P1	P2	P3
GGA	1.90	2.20 (2.62) ^a	1.57	1.43	1.54
GW	3.38	3.86 (4.32) ^a	2.62	2.42	2.52
GW [44]	3.59	3.83 (4.29) ^a			
GW [45]	3.34	3.56			
GW [46]	3.46	3.73			
GW [47]	3.40	3.70			
GW [48]	3.23				
GW [49]	3.13				
PES [9]	3.6 ± 0.2				
Opt. [6,11]	3.05	3.2			

^aDirect gap at the Γ point.

CBM and VBM of Ti_nN₂O_{2n-3} compounds are predicted to match better with the water-splitting levels.

V. SUMMARY

We have studied Ti oxynitrides with a composition of Ti_nN₂O_{2n-3} that have much higher nitrogen concentrations compared to conventional N-doped Ti oxides. We demonstrate, through first-principles calculations, that Ti_nN₂O_{2n-3} compounds can be promising materials to achieve better photocatalytic performance for splitting water. In particular, corundum-type Ti₂N₂O, an example Ti_nN₂O_{2n-3} compound, is found to have a small band gap that is suitable to absorb visible light. The band-edge potentials of Ti₂N₂O are much better aligned to the water reduction and oxidation levels. We anticipate the synthesis of Ti_nN₂O_{2n-3} structures and their applications for visible-light-driven water-splitting photocatalytic systems.

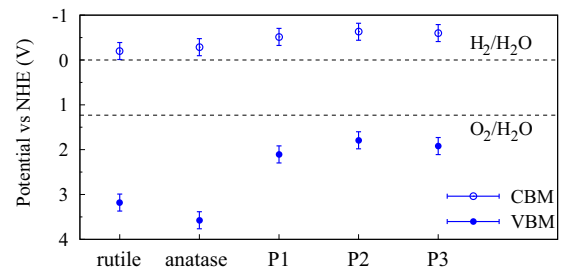


FIG. 6. Estimated GW CBM and VBM positions relative to the water reduction and oxidation levels for pristine TiO₂ phases (rutile and anatase) and corundum-based Ti₂N₂O structures (P1–P3).

ACKNOWLEDGMENTS

Y.A. and S.S. acknowledge support from the MEXT Japan Elements Strategy Initiative to Form Core Research Center, JSPS KAKENHI Grant No. JP25107005, and JSPS Grant No. JP14J11856. S.C., S.G.L., and M.L.C. acknowledge support by the National Science Foundation (NSF) Grant No. DMR-1508412 (which provided the DFT calculations), and the Theory of Materials Program at the Lawrence Berkeley National Laboratory (LBNL) funded by the Director, Office of Science, Basic Energy Sciences, Materials Sciences and Engineering Division, U.S. Department of Energy (DOE) under Contract No. DE-AC02-05CH11231 (which provided the GW calculations). Advanced codes were provided by the Center for Computational Study of Excited-State Phenomena in Energy Materials (C2SEP) at LBNL, which is funded by the U.S. DOE, Office of Science, Basic Energy Sciences, Materials Sciences and Engineering Division under Contract No. DE-AC02-05CH11231, as part of the Computational Materials Sciences Program. M.S. and J.R.C. are supported by the same under a subcontract for algorithm development. They also acknowledge support from the U.S. DOE for work on complex materials and nanostructures from Grant No. DE-FG02-06ER46286. HPC resources were provided by the National Energy Research Scientific Computing Center (NERSC).

- [1] A. L. Linsebigler, G. Lu, and J. T. Yates, *Chem. Rev.* **95**, 735 (1995).
- [2] X. Chen and S. S. Mao, *Chem. Rev.* **107**, 2891 (2007).
- [3] K. Nakata, T. Ochiai, T. Murakami, and A. Fujishima, *Electrochim. Acta* **84**, 103 (2012).
- [4] A. Fujishima and K. Honda, *Nature (London)* **238**, 37 (1972).
- [5] K. Hashimoto, H. Irie, and A. Fujishima, *Jpn. J. Appl. Phys.* **44**, 8269 (2005).
- [6] D. C. Cronmeyer, *Phys. Rev.* **87**, 876 (1952).
- [7] J. Pascual, J. Camassel, and H. Mathieu, *Phys. Rev. B* **18**, 5606 (1978).
- [8] Y. Tezuka, S. Shin, T. Ishii, T. Ejima, S. Suzuki, and S. Sato, *J. Phys. Soc. Jpn.* **63**, 347 (1994).
- [9] S. Rangan, S. Katalinic, R. Thorpe, R. A. Bartynski, J. Rochford, and E. Galoppini, *J. Phys. Chem. C* **114**, 1139 (2010).
- [10] H. Tang, F. Lévy, H. Berger, and P. E. Schmid, *Phys. Rev. B* **52**, 7771 (1995).
- [11] N. Hosaka, T. Sekiya, C. Satoko, and S. Kurita, *J. Phys. Soc. Jpn.* **66**, 877 (1997).
- [12] R. Asahi, T. Morikawa, T. Ohwaki, K. Aoki, and Y. Taga, *Science* **293**, 269 (2001).
- [13] S. Livraghi, M. C. Paganini, E. Giamello, A. Selloni, C. Di Valentin, and G. Pacchioni, *J. Am. Chem. Soc.* **128**, 15666 (2006).
- [14] Y. Aoki and S. Saito, *J. Ceram. Soc. Jpn.* **121**, 373 (2013).
- [15] M. Batzill, E. H. Morales, and U. Diebold, *Phys. Rev. Lett.* **96**, 026103 (2006).
- [16] A. K. Rumaiz, J. C. Woicik, E. Cockayne, H. Y. Lin, G. H. Jaffari, and S. I. Shah, *Appl. Phys. Lett.* **95**, 262111 (2009).
- [17] P. Hohenberg and W. Kohn, *Phys. Rev.* **136**, B864 (1964).
- [18] W. Kohn and L. J. Sham, *Phys. Rev.* **140**, A1133 (1965).

- [19] M. S. Hybertsen and S. G. Louie, *Phys. Rev. B* **34**, 5390 (1986).
- [20] P. Giannozzi *et al.*, *J. Phys.: Condens. Matter* **21**, 395502 (2009).
- [21] J. P. Perdew, K. Burke, and M. Ernzerhof, *Phys. Rev. Lett.* **77**, 3865 (1996).
- [22] N. Troullier and J. L. Martins, *Phys. Rev. B* **43**, 1993 (1991).
- [23] H. J. Monkhorst and J. D. Pack, *Phys. Rev. B* **13**, 5188 (1976).
- [24] R. H. Byrd, P. Lu, J. Nocedal, and C. Zhu, *SIAM J. Sci. Comput.* **16**, 1190 (1995).
- [25] C. Zhu, R. H. Byrd, P. Lu, and J. Nocedal, *ACM Trans. Math. Software* **23**, 550 (1997).
- [26] J. L. Morales and J. Nocedal, *ACM Trans. Math. Software* **38**, 1 (2011).
- [27] S. B. Zhang, D. Tománek, M. L. Cohen, S. G. Louie, and M. S. Hybertsen, *Phys. Rev. B* **40**, 3162 (1989).
- [28] J. Deslippe, G. Samsonidze, D. A. Strubbe, M. Jain, M. L. Cohen, and S. G. Louie, *Comput. Phys. Commun.* **183**, 1269 (2012).
- [29] G. Samsonidze, M. Jain, J. Deslippe, M. L. Cohen, and S. G. Louie, *Phys. Rev. Lett.* **107**, 186404 (2011).
- [30] J. Deslippe, G. Samsonidze, M. Jain, M. L. Cohen, and S. G. Louie, *Phys. Rev. B* **87**, 165124 (2013).
- [31] R. E. Newnham and Y. M. de Haan, *Z. Kristallogr.* **117**, 235 (1962).
- [32] S. Åsbrink and A. Magnéli, *Acta Crystallogr.* **12**, 575 (1959).
- [33] R. F. Bartholomew and D. R. Frankl, *Phys. Rev.* **187**, 828 (1969).
- [34] M. Taguchi, A. Chainani, M. Matsunami, R. Eguchi, Y. Takata, M. Yabashi, K. Tamasaku, Y. Nishino, T. Ishikawa, S. Tsuda, S. Watanabe, C.-T. Chen, Y. Senba, H. Ohashi, K. Fujiwara, Y. Nakamura, H. Takagi, and S. Shin, *Phys. Rev. Lett.* **104**, 106401 (2010).
- [35] See Supplemental Material at <http://link.aps.org/supplemental/10.1103/PhysRevB.99.075203> for atomic positions of $\text{Ti}_2\text{N}_2\text{O}$ structures.
- [36] S. C. Abrahams and J. L. Bernstein, *J. Chem. Phys.* **55**, 3206 (1971).
- [37] M. Horn, C. F. Schwerdtfeger, and E. P. Meagher, *Z. Kristallogr.* **136**, 273 (1972).
- [38] A. Marzouk, H. Bolvin, P. Reinhardt, L. Manceron, J. P. Perchard, B. Tremblay, and M. E. Alikhani, *J. Phys. Chem. A* **118**, 561 (2014).
- [39] Y. Wu, P. Lazic, G. Hautier, K. Persson, and G. Ceder, *Energy Environ. Sci.* **6**, 157 (2013).
- [40] G. Hyett, M. A. Green, and I. P. Parkin, *J. Am. Chem. Soc.* **129**, 15541 (2007).
- [41] A. Salamat, G. Hyett, R. Q. Cabrera, P. F. McMillan, and I. P. Parkin, *J. Phys. Chem. C* **114**, 8546 (2010).
- [42] M. Mikami and K. Ozaki, *J. Phys.: Conf. Ser.* **379**, 012006 (2012).
- [43] M. K. Y. Chan and G. Ceder, *Phys. Rev. Lett.* **105**, 196403 (2010).
- [44] L. Chiodo, J. M. García-Lastra, A. Iacomino, S. Ossicini, J. Zhao, H. Petek, and A. Rubio, *Phys. Rev. B* **82**, 045207 (2010).
- [45] W. Kang and M. S. Hybertsen, *Phys. Rev. B* **82**, 085203 (2010).
- [46] M. Landmann, E. Rauls, and W. G. Schmidt, *J. Phys.: Condens. Matter* **24**, 195503 (2012).
- [47] C. E. Patrick and F. Giustino, *J. Phys.: Condens. Matter* **24**, 202201 (2012).
- [48] G. Samsonidze, C.-H. Park, and B. Kozinsky, *J. Phys.: Condens. Matter* **26**, 475501 (2014).
- [49] A. Malashevich, M. Jain, and S. G. Louie, *Phys. Rev. B* **89**, 075205 (2014).
- [50] Y. Wu, M. K. Y. Chan, and G. Ceder, *Phys. Rev. B* **83**, 235301 (2011).